RAA 2014 Vol. **14** No. **11**, 1469–1480 doi: 10.1088/1674–4527/14/11/010
http://www.raa-journal.org *http://www.iop.org/journals/raa*

Research in Astronomy and Astrophysics

Some tests and improvements to the VFISV: Very Fast Inversion of the Stokes Vector for the Helioseismic and Magnetic Imager *

Fei Teng and Yuan-Yong Deng

Key Laboratory of Solar Activity, National Astronomical Observatories, Chinese Academy of Sciences, Beijing 100012, China; *fteng@bao.ac.cn, dyy@bao.ac.cn*

Received 2013 December 9; accepted 2014 May 4

Abstract Some experimental tests and improvements to the Very Fast Inversion of the Stokes Vector program, which is designed for the inversion calculation used by the Helioseismic and Magnetic Imager instrument on the *Solar Dynamics Observatory*, are given. On one hand, the interpolation for calculating the Voigt function is not smooth, which may occasionally cause the iteration process to converge to different minima although they are very close to initial values. This problem can be solved by a smoother interpolation. On the other hand, in order to improve the performance of this program, we have tried to abandon the randomly-jump-out strategy and set the initial value properly to avoid non-global minima. The resulting method costs only $1/4$ of the computational time, and will be very competitive when the users are only interested in the vectorial magnetic fields and the velocities along the line of sight.

Key words: Sun: magnetic fields — methods: numerical — techniques: polarimetric

1 INTRODUCTION

The Helioseismic and Magnetic Imager (HMI) is an instrument on the *Solar Dynamics Observatory* for the purpose of studying solar magnetic fields, which are very important for understanding the radiation, revolution and the essence of many solar activities (Schou et al. 2012). One of the cameras in this platform can capture full-disk images of Stokes (I, Q, U, V) parameters at 4096×4096 pixels. Based on this instrument, reliable determination of the magnetic fields and other thermodynamic parameters in the solar atmosphere through the Stokes parameters is the main task of the data processing system.

Historically, Harvey et al. (1971) used the Milne-Eddington (M-E) solar atmosphere model to calculate the solar magnetic fields considering only the Stokes I and V for the first time. They did not consider the Faraday magneto-optic effect yet. Auer et al. (1977) considered all the four Stokes parameters. They used the Levenberg-Marquardt (L-M) algorithm, which was also used by most of the later inversion procedures. Then Landolfi et al. (1984) generalized this method to include the magneto-optic and damping effect, and Skumanich & Lites (1987) proposed another free parameter to depict the influence of stray light. However, this technique was also used by Lites et al. (1988) to deal with chromospheric situations. Notice that all the above developments are based on the non-linear least squares method and the hypothesis that the magnetic fields and speed along the

* Supported by the National Natural Science Foundation of China.

line of sight are constant along the optical depth. After 1990, some other models and algorithms were considered. Some researchers used the flux tube model and other MHD limitations as extra conditions during the inversion process, including Sanchez Almeida et al. (1996); Sanchez Almeida (1997); Bellot Rubio et al. (1997); Frutiger & Solanki (1998); Bellot Rubio et al. (2000a,b). Others considered non-iterative methods such as principal component analysis (Rees et al. 2000; Socas-Navarro et al. 2001) and artificial neural networks (Carroll & Staude 2001). They could obtain the inversion results very quickly, depending on the training database established in advance.

The Very Fast Inversion of the Stokes Vector (VFISV) is a program that performs inversion calculations for the radiative transfer equations especially designed for HMI (Borrero et al. 2011). To achieve a compromise between speed and accuracy, the traditional M-E solar atmosphere model and a modified L-M non-linear least squares method (Landolfi & Landi Degl'Innocenti 1982) are used. The analytical solution to the simplified model can not only significantly speed up the procedure to synthesize profiles, but also speed up calculating the derivatives of Stokes parameters with respect to the model parameters such as magnetic fields.

Although this synthesis model is almost the simplest one of many solar atmosphere models, because of the relatively low spectral resolution of the HMI instrument (six points), the inversion problem seems not well defined in a few cases according to the result for some real data. Some sharp points are discernable in some resulting images of the inversion calculation, which are relatively smooth in the original images of the Stokes parameters. It is believed that even with a small difference in initial values, the iteration may converge to different local minima. For decreasing the probability of falling into a local minimum which is considered to be an error, a randomly perturbed model is used in VFISV. If bad attempts in the L-M algorithm (Moré 1978) continue several times, the program randomly chooses a direction and a big step to jump out of the local minimum and restarts the iteration. In computations applied to real data, this strategy can really decrease the number of sharp points, but it cannot eliminate all of them.

In this paper, we found that first-order non-continuous interpolation, which is used in the algorithm for VFISV to calculate Voigt functions, is a major reason for some sharp points. If a smoother interpolation based on cubic polynomials is used to calculate the Voigt functions, these sharp points in the magnetic fields are eliminated.

In order to implement a more efficient algorithm, we also tried to avoid jumping out when the algorithm cannot find an available step by setting multiple initial values for the azimuth angles ϕ of the magnetic fields, and choosing the results with minimal objective functions χ^2 in the least squares problem. The new method may leave many non-convergent points and cannot replace the randomly-jump-out strategy, but it can save about $3/4$ of the time. According to our experience, the obtained results are adequate if the user is only interested in the vectorial magnetic fields and the velocities along the line of sight.

A brief description and tests demonstrating the advantages of the VFISV compared to the classical L-M algorithm will be given in Section 2, and we will discuss our tests and improvements in Section 3. Finally, we will provide conclusions and discussion in Section 4.

2 STOKES INVERSION ALGORITHM OF VFISV

According to the radiation transfer equations of Stokes parameters as described in Borrero (2004) or Landi Degl'Innocenti (1976), we can obtain the synthesized I, Q, U and V profiles related to p and λ, i.e. $f_i\,(p, \lambda)$, where index $i = 1, \ldots, 4$ stands for I, Q, U and V respectively. p stands for eight parameters in the solar atmosphere model, including

(1) Magnitude of the magnetic field B;
(2) Doppler broadening $\Delta\lambda_{\rm D}$;
(3) Velocity along the line of sight $v_{\rm los}$;
(4) Angle ψ between the magnetic field and the line of sight (axis z);

(5) Angle ϕ between the projection from the magnetic field onto $x-y$ plane and axis x;
(6) Ratio between the fictitious absorption coefficient at the line center and the continuous extinction coefficient at the reference wavelength η_0;
(7) Parameter S_0 in the representation of the Planck function;
(8) Parameter S_1 in the representation of the Planck function,

except the damping a, which is considered to be a constant 0.5 during the inversion process, and λ stands for the observed wavelength. For the computation that is applied to the observed data from HMI, the filter's profile of the instrument must also be considered. If we let $s_{ij}(\lambda)$ represent such profiles, where index i shares the same meaning as above, and index $j = 1, \ldots, m$ denotes different filters, because $m = 6$ is for HMI, whose filter's profiles are illustrated in Figure 1, the synthesized profiles behind filters can be calculated from

$$F_{ij}(p) = \int_{\lambda} f_i(p, \lambda) s_{ij}(\lambda) d\lambda. \tag{1}$$

Define the objective function of the non-linear least squares problem as

$$\chi^2 = \sum_{i=1}^{4} \sum_{j=1}^{m} \frac{1}{w_i^2} \left[y_{ij} - F_{ij}(p) \right]^2, \tag{2}$$

where y_{ij} are the observed values with index i, j has the same meaning as above and w_i are the weights for different i in order to fit the different scales of I, Q, U and V. The objective is to find a suitable p to obtain the minimum of χ^2. Finally, the algorithm adopted by VFISV (Borrero et al. 2011) can be summarized as

(1) Set initial values for p and initial relaxation parameter τ;
(2) If the total number of iteration steps is larger than the criterion, stop the algorithm and set the result to p where χ^2 achieves its minimal value among all the iteration steps;
(3) Calculate Stokes profiles and their Jacobi matrix $\mathbf{J}$ with respect to p;

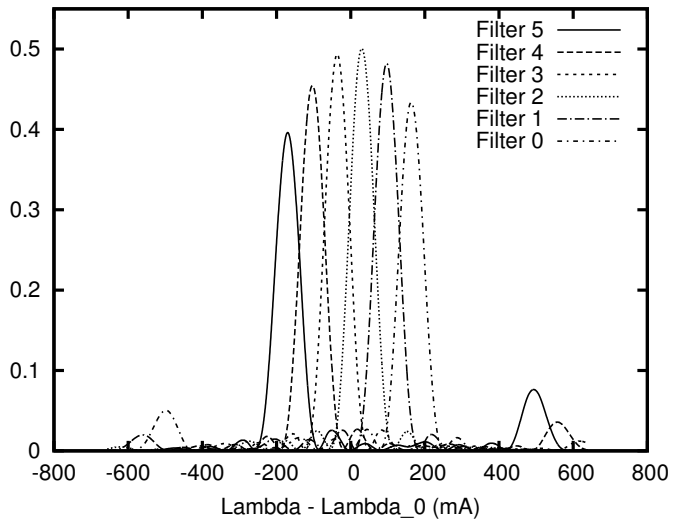

Fig. 1 Filter's Profile of HMI.

(4) Calculate the objective function χ^2 and its gradient g with respect to p;
(5) Solve the linear system of equations $(J^{\mathrm{T}}J + \tau\mathbf{D})s = -g$, where $\mathbf{D}$ is a diagonal matrix with diagonal elements that are the same as $J^{\mathrm{T}}J$;
(6) Set $p^{\mathrm{pre}} = p + s$ and calculate the objective function χ^{pre} with respect to p^{pre},
  (i) If $\chi^{\mathrm{pre}} < \chi$, accept p^{pre} as p, decrease τ, and go to step 2 for the next iteration.
  (ii) If $\chi^{\mathrm{pre}} > \chi$, increase τ, and go to step 2 to calculate s again. If $\chi^{\mathrm{pre}} > \chi$ continuously for several times, then randomly set a step s within a tenable range, replace p with $p + s$, and go to step 2 for the next iteration.

Notice that the above algorithm is different from the classical L-M algorithm. The diagonal of $J^{\mathrm{T}}J$ is used instead of the identity matrix $\mathbf{I}$ in step 2 and in step 2 the condition for increasing τ is simpler than the classical one in which the degree of the 2nd order approximation must be tested. However, a randomly-jump-out strategy is used when τ continuously increases several times.

Actually, these differences change the essence of the classical algorithm. The modified algorithm does not have the global convergence property which the classical one does. Theoretically, wherever we choose the initial point, the classical one can converge to a stable point (the gradient of χ^2 with respect to p is zero), but experiences show that if we abandon the randomly-jump-out strategy, the gradient cannot converge to zero by the modified algorithm with many initial values. However, in our problem, these non-convergent phenomena usually emerge near the minima that we do not want p to converge to, so it is more efficient than the classical algorithm because it does not waste much time near the non-global minima. We can conclude from these tests that the 2rd order approximation usually behaves better near global minima than non-global ones. The shortcoming is that the number of iterations must reach the limit for every calculation.

3 EXPERIMENTAL IMPROVEMENT TO VFISV

3.1 Improve the Smoothness of the Interpolated Voigt Functions

Although the above algorithm is very successful in avoiding non-global minima, among the results calculated by VFISV, we can also find some sharp points in magnetic fields.

Figure 2 is an example. The upper graph shows the magnetic fields strength B from an inversion result. The coordinates in 2D space $x - y$ are expressed in terms of pixels. We can see one of the sharp points at $(x, y) = (126, 70)$ in the red box. The lower diagram illustrates B along the line with $y = 70$.

Through many experiences, we found that the problem exists in the Voigt function $H(a, \nu)$ and $F(a, \nu)$. For calculating Voigt functions, Reichel (1968) proposed a classical and accurate algorithm. But for efficiency, Borrero et al. (2011) proposed an algorithm based on Taylor expansions which is much faster than the classical one, due to the representation of the derivatives (Del Toro Iniesta & Ruiz Cobo 1996)

$$\begin{aligned}
\frac{\partial H(a,\nu)}{\partial a} &= -\frac{\partial F(a,\nu)}{\partial \nu} \\
&= -\frac{2}{\sqrt{\pi}} + 2aH(a,\nu) + 2\nu F(a,\nu) \\
&:= \alpha \qquad (3) \\
\frac{\partial H(a,\nu)}{\partial \nu} &= \frac{\partial F(a,\nu)}{\partial a} \\
&= 2aF(a,\nu) - 2\nu H(a,\nu) \\
&:= \beta, \qquad (4)
\end{aligned}$$

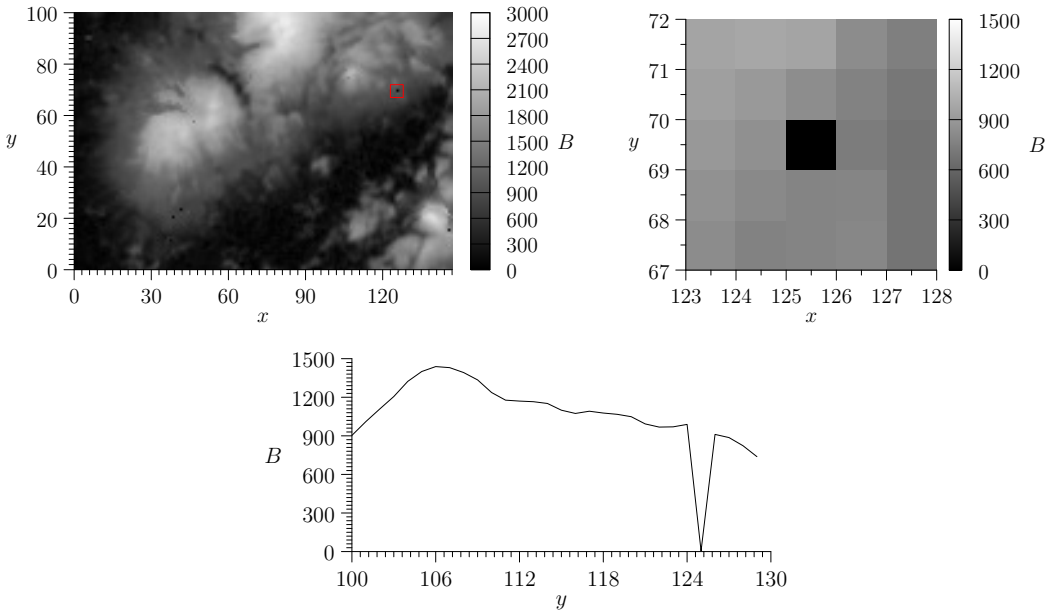

Fig. 2 Sharp points in magnetic fields calculated by VFISV; *Top panels*: Magnetic field strength in 2D space $x - y$ (expressed in terms of pixels); *Bottom panels*: The relation between B and x along the line with $y = 70$.

and

$$\begin{aligned}\frac{\partial^2 H(a,\nu)}{\partial a^2} &= -\frac{\partial^2 H(a,\nu)}{\partial \nu^2} = -\frac{\partial^2 F(a,\nu)}{\partial a \partial \nu} \\ &= 2H(a,\nu) + 2a\alpha + 2\nu\beta, \qquad (5)\\ \frac{\partial^2 F(a,\nu)}{\partial a^2} &= -\frac{\partial^2 F(a,\nu)}{\partial \nu^2} = \frac{\partial^2 H(a,\nu)}{\partial a \partial \nu} \\ &= 2F(a,\nu) + 2a\beta - 2\nu\alpha. \qquad (6)\end{aligned}$$

based on a pre-calculated value at some grid point in the (a, ν) plane, and the approximate Taylor formulae

$$\begin{aligned}H(a+\Delta a, \nu+\Delta\nu) &\simeq H(a,\nu) + \alpha\Delta a + \beta\Delta\nu \\ &\quad + [H(a,\nu) + a\alpha + \nu\beta]\left(\Delta a^2 - \Delta u^2\right) \\ &\quad + 2\left[F(a,\nu) + a\beta - \nu\alpha\right]\Delta a\Delta\nu, \qquad (7)\\ F(a+\Delta a, \nu+\Delta\nu) &\simeq F(a,\nu) + \beta\Delta a - \alpha\Delta\nu \\ &\quad + [F(a,\nu) + a\beta - \nu\alpha]\left(\Delta a^2 - \Delta u^2\right) \\ &\quad - 2\left[H(a,\nu) + a\alpha + \nu\beta\right]\Delta a\Delta\nu, \qquad (8)\end{aligned}$$

or the simpler ones,

$$\begin{aligned}H(a+\Delta a, \nu+\Delta\nu) &\simeq H(a,\nu) + \alpha\Delta a + \beta\Delta\nu\,, \qquad (9)\\ F(a+\Delta a, \nu+\Delta\nu) &\simeq F(a,\nu) + \beta\Delta a - \alpha\Delta\nu. \qquad (10)\end{aligned}$$

The values of H and F at each point in the (a, ν) plane can be obtained by this algorithm.

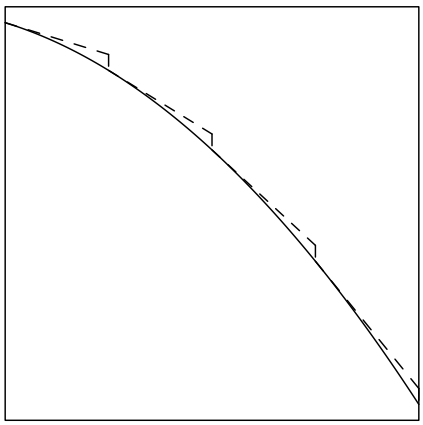

Fig. 3 A non-continuous interpolation.

Actually, in the synthesized model for the VFISV, the damping parameter a is fixed, so only one-dimensional (dimension ν) interpolation is needed. Notice also that for accuracy, the interpolation is only used for $\|\nu\| > 1$ and in the field that has $\|\nu\| < 1$, the more accurate method by Reichel is used. However, we have noticed that the above interpolation can lead to a non-continuous function with respect to ν, because the constant derivatives are used in the whole grid, as illustrated in Figure 3.

In order to improve the smoothness of the resulting function, we try a cubic interpolation instead, that is find a cubic polynomial at each grid (ν_i, ν_{i+1}), such that the function values and its derivatives at the grid vertices coincide with Equations (3) and (4). In detail, let v_i stand for the value of H or F at point (a, ν_i), v_i^ν represent the derivatives of H or F with respect to ν, also at point (a, ν_i), and

$$A = \begin{bmatrix} 1 & 0 & -3 & 2 \\ 0 & 0 & 3 & -2 \\ 0 & 1 & -2 & 1 \\ 0 & 0 & -1 & 1 \end{bmatrix}, \tag{11}$$

$$\xi = \frac{\nu - \nu_i}{\nu_{i+1} - \nu_i},$$

then the interpolated polynomial can be written as

$$Z(a, \nu) = \left[v_i, v_{i+1}, v_i^\nu, v_{i+1}^\nu\right] \cdot A \cdot \begin{bmatrix} 1 \\ \xi \\ \xi^2 \\ \xi^3 \end{bmatrix}, \tag{12}$$

where Z signifies H or F, and $\nu \in (\nu_i, \nu_{i+1})$. Notice that the interpolation by third order polynomials can lead to a continuous derivative of the function Z with respect to ν in the whole area.

Following this improvement, we can see the inversion results from Figure 4 in which the graphs are arranged in the same order as in Figure 3, and the sharp points disappear. More accurately, a scatter diagram in Figure 5 illustrates the difference between the original and improved algorithm. We can easily identify the correction of the sharp points in this diagram. Also notice that the additional time cost by the new interpolation can be ignored when compared with the procedures for calculating the derivatives.

As another demonstration, the original and improved algorithms are also tested based on a simulated database. We synthesize 3000 examples for randomly-set physical parameters in the ranges as

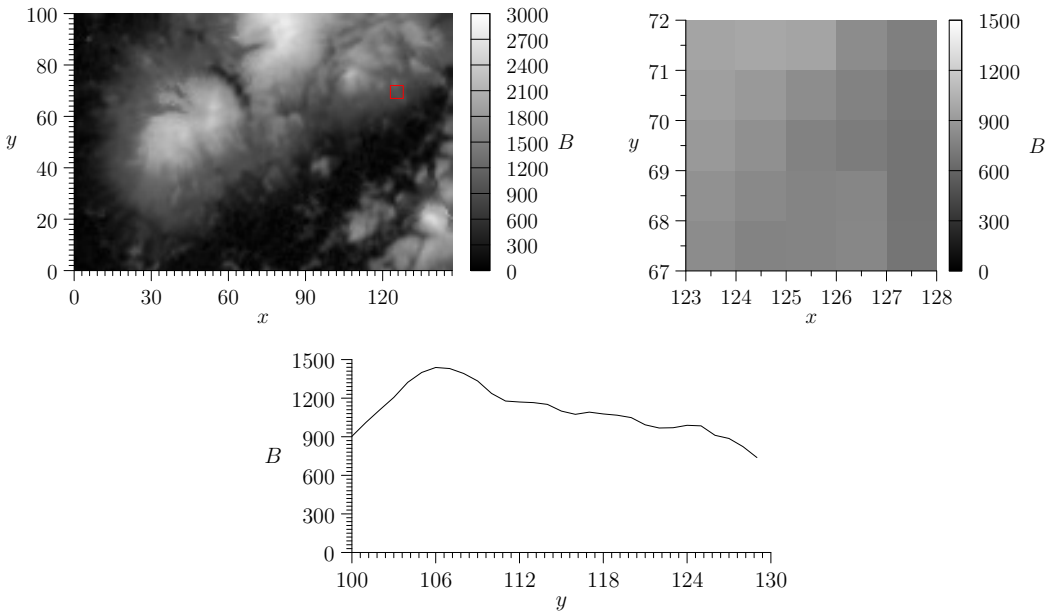

Fig. 4 Sharp points disappear in magnetic fields when cubic interpolation is applied. *Upper panels*: magnetic field strength in 2D space $x - y$ (expressed in terms of pixels); *Lower panel*: The relation between B and x along the line with $y = 70$.

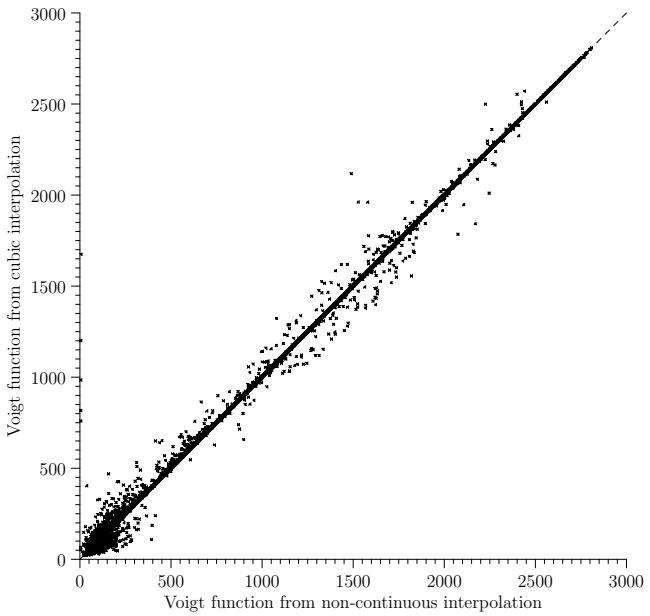

Fig. 5 Scatter diagram to show the comparison in the results between the non-continuous and cubic interpolation for calculating Voigt functions.

Table 1 Ranges of Randomly-set Physical Parameters Used for Testing

Phy. Para.	Lower Limit	Upper Limit
B (G)	200	5000
$\Delta\lambda_{\rm D}$ (cm)	5×10^{-11}	5×10^{-10}
$v_{\rm los}$ (cm s^{-1})	-3×10^5	3×10^5
ψ ($^\circ$)	15	165
ϕ ($^\circ$)	0	180
η_0	5	100
S_0	3000	8000
S_1	3000	8000

Table 2 Average Error between the Known and Inverted Physical Parameters for the Randomly-set Database

Phy. Para.	Cubic Inter.	Non-continuous Inter.
B (G)	1.30×10^2	7.28×10^2
$\Delta\lambda_{\rm D}$ (cm)	4.27×10^{-11}	2.02×10^{-10}
$v_{\rm los}$ (cm s^{-1})	5.98×10^3	2.47×10^4
ψ (rad)	4.25×10^{-2}	2.20×10^{-1}
ϕ (rad)	1.31×10^{-1}	3.58×10^{-1}
η_0	2.37×10^1	4.74×10^1
S_0	1.95×10^2	1.37×10^3
S_1	2.55×10^2	1.49×10^3

shown in Table 1, and add additional errors that follow a normal distribution $N(0, 50)$ to the Stokes parameters. For accuracy, we use four-point Gaussian quadrature to calculate each Voigt function when constructing the database.

Then, by applying the original and improved algorithms to this database, we can obtain the average error between the known and inverted physical parameters. Table 2 shows the average error for the original and improved algorithms as a comparison. The cubic interpolation obviously behaves better.

In order to further validate the effect of eliminating the sharp points in magnetic fields, we counted the number of points with an error of B larger than $500\,$G. A total of 957 examples are included in the original interpolation and 69 examples are included in the cubic interpolation.

3.2 Test about Replacement for Randomly-jump-out Strategy

The randomly-jump-out method at step 2 in the above algorithm is very useful to avoid the solution falling into a non-global local minimum during the iteration process. However, it is rather inefficient when applied to real observed data. The number of iterations will reach the limit at every point.

From computational experience, we found that different initial values of the azimuth angles ϕ are very likely to lead to different local minima. We have tried some methods that are alternatives for the randomly-jump-out strategy by setting different initial values of ϕ, in particular by setting ϕ to be $22.5^\circ, 67.5^\circ, 112.5^\circ$ and 157.5° in four repeated calculations respectively (we call this the 4-ϕ method), and choose the solution with the minimal χ^2. In order to make the algorithm more efficient, we also make τ more sensitive with respect to the non-global minima by enlarging τ when the predicted values are not accepted at step 2 in the algorithm. Figure 6 illustrates a comparison between the results from the 4-ϕ method and the original randomly-jump-out strategy.

To demonstrate accuracy, the scatter diagrams of eight parameters that show the comparison between the two methods are illustrated in Figures 7 and 8.

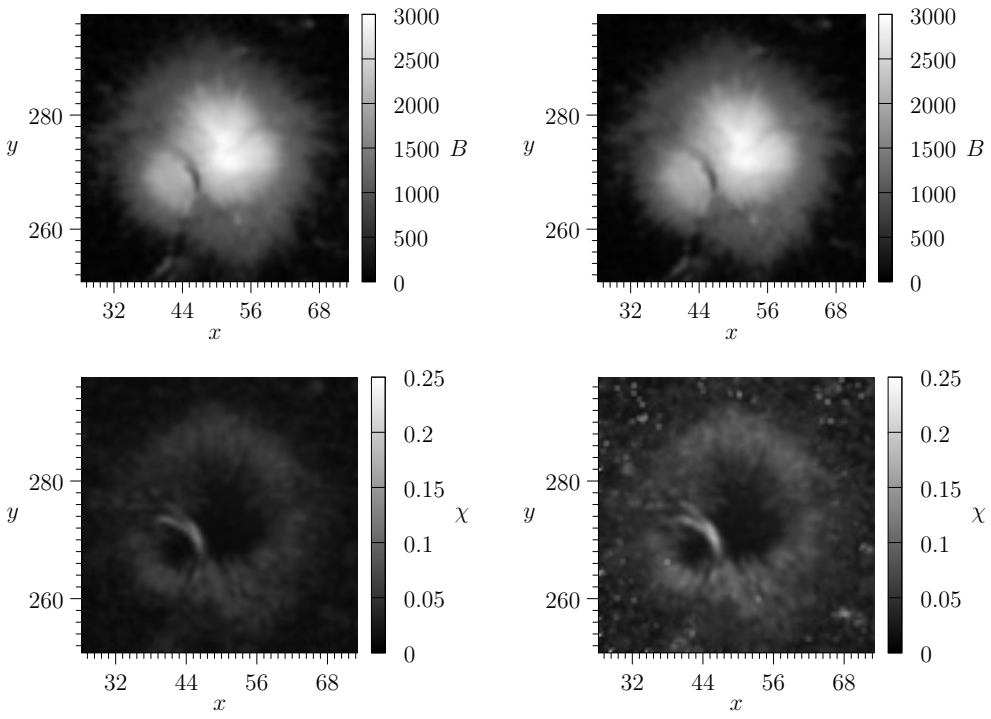

Fig. 6 Comparison between the randomly-jump-out strategy and the multi-initial-value method on AR 11423. *Left*: Results for the randomly-jump-out strategy; *Right*: Results for the multi-initial-value method.

On average, the χ of the new method is about twice as large as the original one, but it only uses a quarter of the time. From these diagrams, we can see that the parameters related to the magnitude of magnetic fields B, and the velocity along the line of sight $v_{\rm los}$ coincide much better than the other parameters; that means the increase of the χ for the new method is mostly caused by the latter four parameters. Four other active regions are also calculated to validate this conclusion. Table 3 shows the respective values for χ error and the computing time.

As in Section 3.1, the same database is used to test the stability of the modification. The results for the average error are listed in Table 4. Notice that in both cases, the Voigt functions are calculated by the above cubic interpolation.

Table 3 χ Error and Computing Time for 4-ϕ and the Random-jump-out Strategy

Active region	4-ϕ strategy		Randomly-jump-out strategy	
	Time used (per pixel)	average of χ	Time used (per pixel)	average of χ
11391	1.92×10^{-3}	5.53×10^{-2}	9.16×10^{-3}	2.89×10^{-2}
11402	1.94×10^{-3}	6.38×10^{-2}	9.11×10^{-3}	3.61×10^{-2}
11401	2.11×10^{-3}	6.18×10^{-2}	8.89×10^{-3}	3.31×10^{-2}
11423	2.11×10^{-3}	5.23×10^{-2}	9.09×10^{-3}	2.85×10^{-2}
11445	1.84×10^{-3}	5.07×10^{-2}	9.03×10^{-3}	2.70×10^{-2}

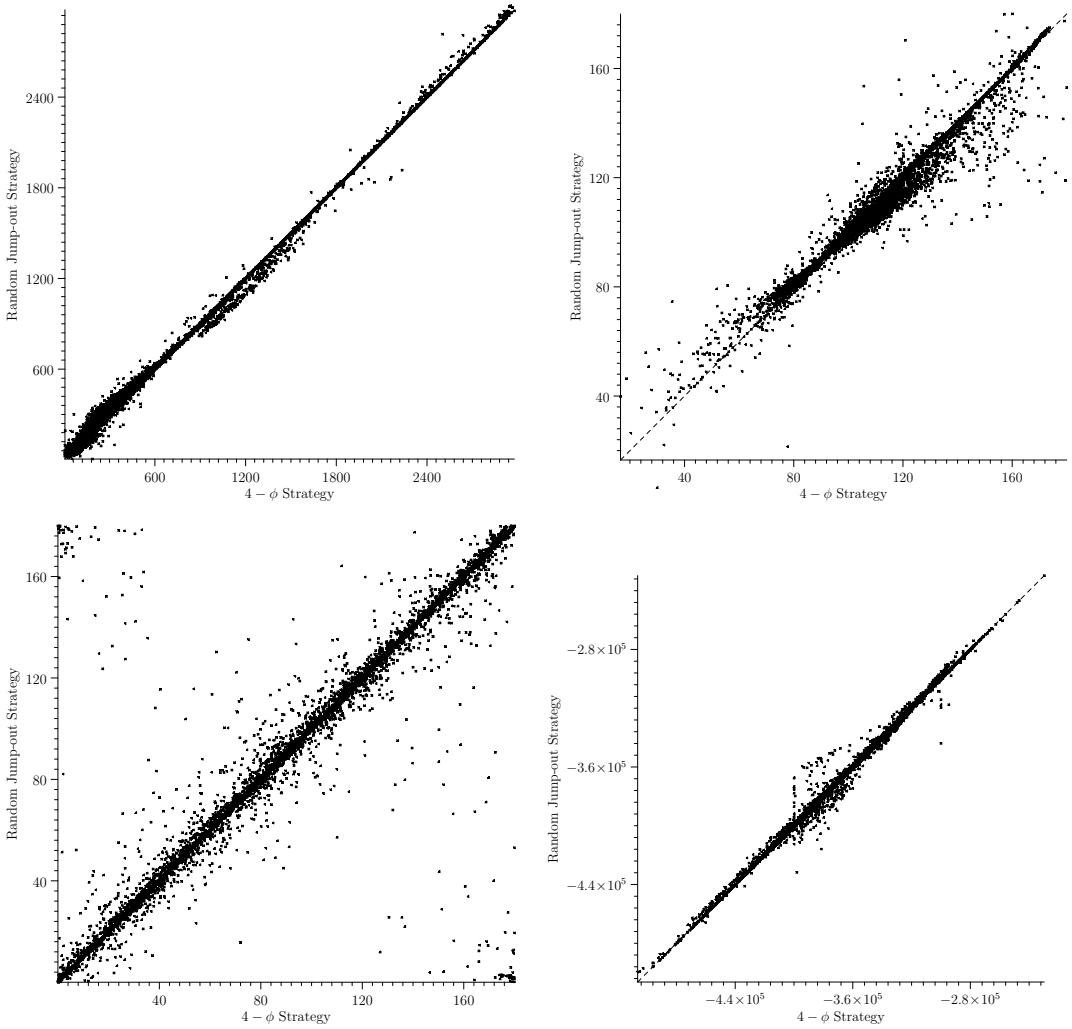

Fig. 7 Scatter diagram to show the comparison between initially setting four different ϕ and using the random-jump-out strategy on AR 11423. Left for b and ϕ; Right for ψ and $v_{\rm los}$.

Table 4 Average Error between the Known and Inverted Physical Parameters for the Randomly-set Database

Phy. Para.	Randomly-jump	4-ϕ
B (G)	1.42×10^{2}	1.82×10^{2}
$\Delta\lambda_{\rm D}$ (cm)	4.43×10^{-11}	6.26×10^{-11}
$v_{\rm los}$ (cm s^{-1})	6.72×10^{3}	8.01×10^{3}
ψ (rad)	4.32×10^{-2}	4.54×10^{-2}
ϕ (rad)	1.42×10^{-1}	1.51×10^{-1}
η_0	2.38×10^{1}	2.50×10^{1}
S_0	2.15×10^{2}	5.41×10^{2}
S_1	2.77×10^{2}	6.57×10^{2}

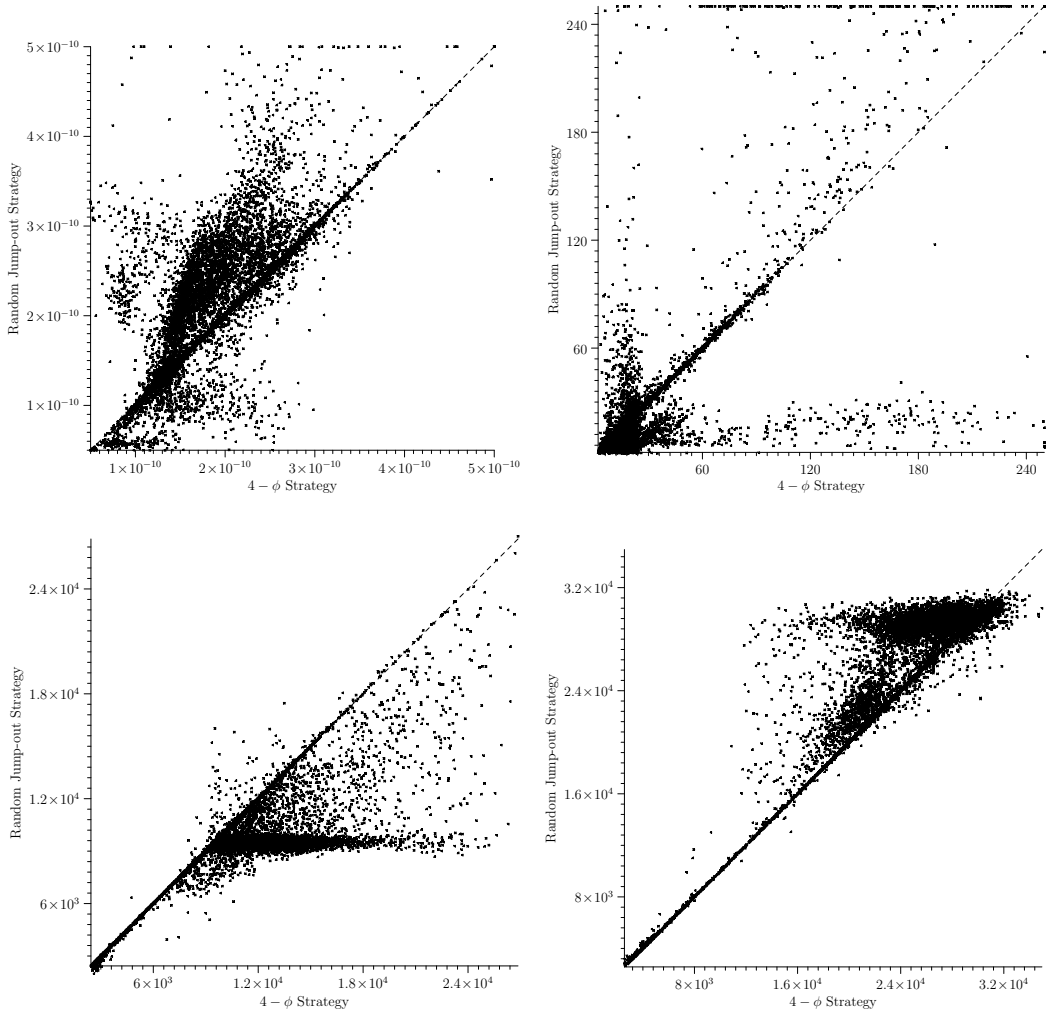

Fig. 8 Same as Fig. 7 but left for $\Delta\lambda_D$ and S_0; right for η_0 and S_1.

From the above results, the 4-ϕ strategy costs only $1/4$ of the computing time as the randomly-jump-out strategy, but the results of the two methods did not coincide at some points in which the iterations with the 4-ϕ strategy led to larger χ errors. These results show the test is not completely successful and the strategy we have tried cannot replace the randomly-jump-out strategy yet.

4 CONCLUSIONS AND DISCUSSION

VFISV is a program designed to obtain Stokes inversion results very fast. However, because of the low spectral resolution of the HMI instrument, the reliability of the non-linear least squares problem can be questioned. In other words, the objective function χ^2 with respect to the parameters p is not always convex in the whole computational domain. The randomly-jump-out strategy (Sect. 2) is used to find the global minimum of the problem. It can reduce most of the sharp points which seem to be caused by instability in the resulting images, but it cannot eliminate all of them.

First, we found that the interpolation for calculating Voigt functions in the VFISV is not smooth. When we change it to the interpolation by a third order polynomial, these sharp points in B disappear (Sect. 3.1).

We also tested another initial value strategy by setting different ϕ, which is simpler than the original randomly-jump-out strategy. On average, it can reduce about $3/4$ of the computing time (Sect. 3.2), and yield almost the same results as the randomly-jump-out strategy for parameters B, ψ, ϕ and $v_{\rm los}$. However, it cannot replace the randomly-jump-out strategy yet because the least-square errors χ obtained from the new method are also about twice as large as from the original one. When the users are only interested in these four parameters, it is a competitive substitution.

Acknowledgements We would like to thank the National Natural Science Foundation of China (Grant Nos. 11178005 and 11221063), the Knowledge Innovation Project of the Chinese Academy of Sciences (CAS, KJCX2-EW-T07), instrument related project, and XDA04060804-02 for the funding support to our work.

References

Auer, L. H., House, L. L., & Heasley, J. N. 1977, Sol. Phys., 55, 47
Bellot Rubio, L. R., Ruiz Cobo, B., & Collados, M. 1997, ApJ, 478, L45
Bellot Rubio, L. R., Ruiz Cobo, B., & Collados, M. 2000a, ApJ, 535, 475
Bellot Rubio, L. R., Ruiz Cobo, B., & Collados, M. 2000b, ApJ, 535, 489
Borrero, J. M., Tomczyk, S., Kubo, M., et al. 2011, Sol. Phys., 273, 267
Borrero, J. M. 2004, The Fine Structure of the Sunspot Penumbra, Ph.D. Thesis, Universität zu Göttingen
Carroll, T. A., & Staude, J. 2001, A&A, 378, 316
Del Toro Iniesta, J. C., & Ruiz Cobo, B. 1996, Sol. Phys., 164, 169
Frutiger, C., & Solanki, S. K. 1998, A&A, 336, L65
Harvey, J., Livingston, W. L., & Slaughter, C. 1971, Line Formation in the Presence of Magnetic Fields, Manuscripts Presented at a Conference Held in Boulder
Landi Degl'Innocenti, E. 1976, A&AS, 25, 379
Landolfi, M., & Landi Degl'Innocenti, E. 1982, Sol. Phys., 78, 355
Landolfi, M., Landi Degl'Innocenti, E., & Arena, P. 1984, Sol. Phys., 93, 269
Lites, B. W., Skumanich, A., Rees, D. E., & Murphy, G. A. 1988, ApJ, 330, 493
Moré, J. J. 1978, The Levenberg-Marquardt Algorithm: Implementation and Theory, in Lecture Notes in Mathematics 630: Numerical analysis, ed. Watson, G. A., 105 (Berlin: Springer-Verlag)
Rees, D. E., López Ariste, A., Thatcher, J., & Semel, M. 2000, A&A, 355, 759
Reichel, A. 1968, J. Quant. Spec. Radiat. Transf., 8, 1601
Sanchez Almeida, J., Landi Degl'Innocenti, E., Martinez Pillet, V., & Lites, B. W. 1996, ApJ, 466, 537
Sanchez Almeida, J. 1997, ApJ, 491, 993
Schou, J., Borrero, J. M., Norton, A. A., et al. 2012, Sol. Phys., 275, 327
Skumanich, A., & Lites, B. W. 1987, ApJ, 322, 473
Socas-Navarro, H., López Ariste, A., & Lites, B. W. 2001, ApJ, 553, 949